Stacking of Polycyclic Aromatic Hydrocarbons as Prototype for Graphene Multilayers, Studied Using DFT Augmented with a Dispersion Term

C. Feng,[1,2] C. S. Lin, [1,3] W. Fan,[2] R. Q. Zhang,[1] and M. A. Van Hove[1]

[1] *Department of Physics and Materials Science, City University of Hong Kong, Hong Kong SAR, P. R. China*
[2] *Technical Institute of Physics and Chemistry, Chinese Academy of Sciences & Graduate School of Chinese Academy of Sciences, Beijing, P. R. China*
[3] *Fujian Institute of Research on the Structure of Matter, Chinese Academy of Sciences, Fuzhou, P. R. China*

Abstract: The interlayer π-π interaction between finite-size models of graphene sheets was investigated by using a density functional theory (DFT) method, augmented with an empirical R^{-6} term for the description of long-range dispersive interaction; these were calibrated by studying the π-π interaction between various benzene dimer configurations and comparing the results with previous calculations. For stacked bilayers (dimers) and multilayers of polyaromatic hydrocarbons, which serve as molecular models of graphene sheets, we found that binding energies and energy gaps are strongly dependent on their sizes, while the stacking order and the number of stacked layers have a minor influence. The remarkably broad variation of the energy gap, ranging from 1.0 to 2.5 eV, due mainly to variation of the model size, suggests the potential of broadband luminescence in the visible range for carbon-based nanomaterials that have π-π interacting.

1. Introduction

The intermolecular π-π interactions[1] play a crucial role in the crystal packing of organic molecules containing aromatic rings,[2,3] the intercalation of certain drug molecules into DNA,[4] the binding affinities of host-guest complexes,[5-7] as well as the three-dimensional structures of biological systems, including proteins and nucleic acids, and their molecular organization and recognition processes.[8-10] The π-π interactions are also of utmost importance for understanding graphene sheets[11] and other carbon-related nanostructures, including hydrogen-terminated graphene nanoribbons (GNRs) with a width confined to a finite nanoscaled size.[12] A single graphene sheet is a planar monolayer of sp^2-bonded carbon atoms arranged on a two-dimensional honeycomb lattice made of hexagonal rings. Thus, graphene sheets can be stacked into bilayers and multilayers by π-π interactions between the neighboring sheets. A graphene bilayer has very unusual electronic properties, such as the anomalous integer quantum Hall effect (IQHE) that significantly changes with respect to a single layer,[13-15] and which can be used to distinguish between a graphene bilayer and a monolayer. In addition, the electronic properties of graphene multilayers vary with the stacking order, and rapidly evolve with the number of layers, approaching the 3D limit of graphite.[16,17]

Planar polycyclic aromatic hydrocarbons (PAHs) with only benzenoid hexagonal rings can be viewed as fragments of a graphene sheet with the peripheral atoms saturated with hydrogen, and thus provide molecular models of graphene sheets and GNRs. Therefore, PAH dimers can serve as model systems for studying the π-π interactions between graphene sheets. Moreover, the PAHs themselves are of great research interest *per se*, since they are widely found in the residues of domestic and natural combustion of coal, wood,

and other organic materials, and their unique electronic properties provide opportunities for novel functionalized nanomaterials and nanodevices.[18] Furthermore, PAHs are also of particular interest in astrophysics since they are found in many interstellar and circumstellar environments in our galaxy.[19]

The π-stacked sp^2 carbon domains similar to graphene multilayers may also exist in luminescent carbon-based materials, such as in amorphous carbon in CVD diamond films where visible broadband luminescence between 1.5 and 2.5 eV has been observed.[20] The luminescence was attributed to the band-tail states caused by the variations in the energy gap of individual sp^2 carbon clusters, due to their difference in size and/or shape.[21] In particular, the confined band-tail states are generated by the existence of stable graphene-like local structures of various sizes and are the main factor for producing efficient, room-temperature luminescence. First-principles calculations of a series of small hexagonal carbon clusters demonstrated that the energy-gap distribution, due to the difference in size, is considerably broad, which was used to explain the broadband feature of luminescence.[21] A graphene sheet is composed of sp^2 hybrid carbon atoms forming hexagonal rings in a monolayer, and can serve as the building unit for all sp^2 carbon materials. Therefore, it is of great interest to further investigate whether multilayers of graphene, GNRs, and similar carbon-based nanostructures relate to an applicable luminescence phenomenon. This issue needs careful scientific research before such materials can be successfully used in device fabrication.

Because of the short time that has elapsed since the discovery of graphene, experimental investigations of its bilayers and multilayers in particular are rather scarce. Liu *et al*[22] studied the edge structures and stacking of thermally treated bilayer graphene by atomically

resolved high-resolution TEM. However, no confirming conclusions have been so far provided. Furthermore, the experimental measurements of weakly binding systems, such as graphene multilayers, often involve assumptions, and the diverse experimental studies yielded apparently contradictory results.[23] In this regard, theoretical investigations should be performed prior to the experiments, and recent studies indeed clarified the unconventional electronic features of few-layer graphenes. By performing density functional theory (DFT) calculations, Latil and Henrard[24], and Aoki and Amawashi[25] demonstrated the effect of the stacking geometry and the number of layers of graphene multilayers on their band structures in the region of the Fermi level. Guinea *et al*[26] reviewed the role of stacking orders in the electronic levels of graphene stacks using the tight binding model. However, they did not discuss the size-dependence of the electronic band structures, and furthermore, the adopted theoretical methods do not explicitly include the π-π interaction between graphene layers. Grimme *et al*[27] and Zhao *et al*[28] reported theoretical computations of π-π interactions of graphene sheet model dimers using DFT methods that were augmented to account for π-π interaction. However, those studies relate only to the geometrical structures and binding energies of the models, and there is no report about the energy gaps of graphene multilayers and their dependence on size, shape and stacking order. To address these issues, in this study, we conducted theoretical calculations of the energetics, geometries, and electronic energy gaps of model bilayers and multilayers of graphene sheets, and explored their dependence on size, stacking order and number of layers.

2. Theoretical Methods and Computational Details

The π-π interactions are the thermodynamic driving forces for the formation of graphene multilayers, and the binding of these π-stacked complexes is primarily due to the dispersion interactions that are a pure electron correlation effect,[29] which requires using a post-Hartree-Fock wave function theory with a large polarized basis set. The most widely used approach for this purpose is the second-order Møller-Plesset (MP2) perturbation theory and coupled cluster calculations with single and double substitutions with noniterative triple excitations [CCSD(T)]. CCSD(T) is considered to be the most accurate method for describing π-π interactions, but imposes severe computational demands, including an $O(N^7)$ behavior, while the less computationally demanding MP2 method strongly overestimates the dispersion interaction. The conventional DFT methods within the Kohn-Sham formulation and with currently available exchange-correlation functionals are usually efficient for dealing with large systems but fail to describe the dispersion interaction, in particular for the long-range component.[30] A pragmatic way to overcome this drawback of DFT is to add to it an empirical van der Waals (vdW) correction of the form R^{-6}, where R is the interatomic distance, to describe the weak interaction between two separated fragments.[31-38]

In this study, a London-type dispersion term, E_{vdW}, with an asymptotic R^{-6} behavior, is added to the Kohn-Sham total energy E_{DFT} for large distances, and a damping of this term with the onset of overlap of the charge density is included (acronym DFT-D). Therefore, the dispersion corrected total energy is

$$E_{DFT-D} = E_{DFT} + E_{vdW} \qquad (1)$$

with the dispersion energy term E_{vdW} defined as the sum of all possible pairwise atomic contributions,

$$E_{vdW} = -s \cdot \sum_{\alpha\beta} f(R_{\alpha\beta}) \cdot C_6^{\alpha\beta} \cdot R_{\alpha\beta}^{-6} . \qquad (2)$$

Here f(R) is the damping function, $C_6^{\alpha\beta}$ are dispersion coefficients, $R_{\alpha\beta}$ are intermolecular distances, and s is a scaling factor. In this study, we used the same damping function and $C_6^{\alpha\beta}$ coefficients as those in ref. 34, which have been implemented into the DFTB method[39] and successfully used to investigate the structures and binding energies of weakly interacting systems.[40,41] These parameters can be easily applied to systems containing any type of atoms. The scaling factor s, which was first proposed by Grimme[31] to adjust the strength of the added dispersion term to each particular functional form, is determined by considering the different amounts of both Pauli repulsion and dispersion within the overlap regime which the functionals cover. Equation (2) and its analytical derivative with respect to nuclear displacement have been implemented in the SIESTA (Spanish Initiative for Electronic Simulations with Thousands of Atoms) code.[42,43] Note that the empirical dispersion term is calculated separately from the DFT calculations; therefore, it is also compatible with any other standard DFT code.

The DFT-D method was first calibrated using the simplest prototype for the π-π interaction of the benzene dimer, because abundant qualitatively accurate data about it are available for reference from the extensive high-level CCSD(T) calculations that represent the current state-of-the-art data.[44-52] The testing procedures are described in detail in another paper.[53] We found that, using the GGA/PBE (Perdew-Burke-Ernzerhof) functional with basis sets of polarized triple-ζ quality (TZP or TZDP), the DFT-D calculations can provide sufficiently accurate equilibrium intermolecular geometries and the corresponding binding energies of various benzene dimer configurations: these are highly consistent with the experimental measurements and previous CCSD(T) calculations. Moreover, the

stabilization order of various configurations predicted by the DFT-D method is identical to the CCSD(T) results. We also showed that a counterpoise (CP) correction for the basis set superposition error (BSSE) is not required within the DFT-D scheme. The results strongly support the contention that our method can be utilized to evaluate the π-π interactions involving larger graphene sheet model dimers and multilayers, which consist of benzenoid hexagonal rings.

In this study, we used PBE functionals for the exchange-correlation interactions. The norm-conserving pseudopotentials (PPs) were obtained within the framework of the ANINIT code.[54] A valence triple-ζ basis set including polarization orbitals (TZDP) was employed, as defined by the SIESTA code. Periodic boundary conditions were applied to a supercell with large enough spacing to avoid spurious interactions between adjacent cells.

As mentioned above, planar PAHs with fused hexagonal rings can provide molecular models of graphene sheets. In this study, to mimic graphene sheets, we adopted the following PAHs with fused-benzene ring structures of D_{2h} or D_{6h} symmetry: $C_{16}H_{10}$ (pyrene), $C_{24}H_{12}$ (coronene), $C_{32}H_{14}$ (ovalene), $C_{42}H_{16}$, $C_{54}H_{18}$, $C_{66}H_{20}$, and $C_{80}H_{22}$, illustrated in Figures 1a-g. The geometric structures of the PAHs were independently fully optimized. For example, the optimized $C_{54}H_{18}$ structure is quite close to graphite, since the average optimized C-C bond length is 1.422 Å, close to the C-C distance of 1.421 Å in graphite.[55] Significant differences from the bulk value are only observed at the outer rim (about 1.37 to 1.43 Å). The optimized PAH monomer structures were used to construct parallel dimers as models for graphene bilayers, and were kept geometrically frozen for the subsequent calculations. The equilibrium intermolecular distances and the corresponding binding energies were obtained via point-by-point optimizations by varying the

intermolecular distances between two PAH monomers and calculating the binding energies at each dimer separation, with the monomer structures kept frozen. Full geometry optimizations were also performed, which supported the idea that the monomers remain nearly rigid in the dimer: all C-C and C-H bond lengths stay within 0.002 Å of their values in the monomer. The comparisons also indicate that such minor variations in the geometries caused negligible variation to the binding energies when using rigid monomers vs fully optimized dimer geometries.

3. Results and Discussion

3.1 Interlayer geometries. In this study, we considered three different stacking orders of two parallel graphene sheet models: (1) Staggered stacking (S, see Figure 2a), which is the most common arrangement observed in natural graphite, and in which one half of the carbon atoms in one monomer lie directly above the carbon atoms in the neighboring layer, while the other half lie over the centers of hexagonal rings in the other monomer; (2) Hexagonal stacking (H, not shown), which appears in graphite intercalated compounds,[56] and in which the atoms in one layer occupy positions directly above the atoms in the other layer; and (3) Parallel-displaced stacking (P, see Figure 2b), which resembles the parallel-displaced configuration of the benzene dimer. For dimers of graphene sheet models with increasing size and three different stacking orders, point-by-point optimizations were performed by systematically changing the interlayer separations and calculating the binding energies. Therefore, the equilibrium interlayer distances and the corresponding binding energies can be derived from the binding energy curve as a function of the intermonomer distance. For the S, H, and P stacking orders, we obtained optimal distances of about 3.61

Å, 3.80 Å, and 3.60 Å, respectively, and these values are almost unchanged when increasing the model sizes. Taking the S-stacked coronene dimer as an example, we obtained an optimal intermonomer distance of 3.60 Å, which is larger than the previous theoretical result of 3.40 Å from MP2/6-31G(d) calculations.[57] However, it is widely known that the MP2 calculation with small basis sets substantially overestimates the attraction and thus underestimates the intermolecular distance, compared with the CCSD(T) calculation. For example, for various benzene dimer configurations, the MP2 calculations yield about 0.1 to 0.2 Å smaller intermonomer distances, compared with CCSD(T) data.[45,46] Moreover, our vertical separations of 3.60 Å for PAH dimers with S and P stacking orders are consistent with the observation that in crystals, many aromatic molecules form stacks with approximately parallel molecular planes separated by 3.4-3.6 Å.[58]

3.2 Binding energies. At the optimal interlayer separations, the corresponding binding energies (per carbon atom) of our graphene sheet model dimers increase with increasing PAH sizes for all three different stacking orders, as shown in Figure 3. It can be anticipated that the binding energy per carbon atom will monotonously decrease until the graphene sheet model is large enough to reproduce the experimental exfoliation energy of graphite. The same tendency of the binding energy of PAH dimers was also found by the previous DFT-D treatment.[27] It was further found that the S and P stackings are more favorable than the H stacking, indicating that the S stacking is most favorable for PAH dimers, which is in agreement with the orientations of two consecutive graphene layers in natural graphite. For the coronene dimer, for example, the calculated binding energies are -22.64, -22.30, and -20.12 kcal/mol for the S, P, and H stacking orders, respectively. The coronene dimer with S stacking is almost isoenergetic with its P stacked structure, with the former slightly lower

in energy, while both of them are about 11% more stable than the H stacked coronene dimer. Furthermore, the binding energy of -22.64 kcal/mol for the S stacked coronene dimer is consistent with the previous DFT|B97-D/TZP calculations,[27] which yield -22.4 kcal/mol. In that prior investigation, the authors considered only D6h-symmetric PAH's dimers as molecular models of graphene bilayers with only staggered stacking order. In this study, however, we consider graphene multilayers with different possible stacking orders and defects, with different shapes of PAHs, as described below. Moreover, in contrast to the prior investigation, the main motivation of this study is to address the issue of luminescence of graphene multilayers by calculating their energy gaps. Furthermore, the method used in this study is also different from previous reports.

It is worth noting, from the point of view of possible applications, that the energy difference between the S and H stacking orders shown in our calculations may influence the behavior of different nanodevices such as bearings or motors.[59]

The effect of multilayer stacking on the binding energy was also investigated. For graphene sheets, in stacks with more than two layers, there are two common stacking orders, as shown in Figures 2c and d. One is the staggered stacking order with the layer sequence ABABAB (Bernal stacking) that exists in the highly oriented pyrolytic graphite, and the other is the rhombohedral stacking order with the sequence ABCABC that has also been observed in different types of graphite. The binding energies of coronene and $C_{54}H_{18}$ trimer and tetramer with ABABAB and ABCABC stacking sequences were calculated and are shown in Table 1. It can be seen that the binding energy per layer was increased by less than 2% for both models when an additional layer was added, indicating that the effect of multilayer stacking is very small. In addition, it can be seen that the ABABAB stacking is

more favorable than the ABCABC sequence, which is in agreement with the fact that the former is the most common arrangement of nearest neighbor layers observed in nature.

Furthermore, stacking defects have been repeatedly observed in natural graphitic samples, and also in epitaxially grown graphene films.[60] The relative rotation between two parallel graphene sheet models will induce several different relative orientations in stacked orders, which correspond to the stacking defects, such as the rotated graphene layer on the bulk (underlying) graphite.[61] Therefore, we investigated the variation of the binding energy of $C_{54}H_{18}$ dimers, with the initial S and H stacking orders, as a function of the relative rotational angle between two monomers, as shown in Figure 4. It can be seen that, for H stacking, the binding energy decreases (more negative) with increasing rotational angle, indicating that the originally H stacked dimer will be stabilized with the appearance of stacking defects. In contrast, the dimer with S stacking will be less stable with the stacking defects, since their binding energy increases (more positive) with increasing rotational angle. Furthermore, the rotational angle of 30° from H stacking corresponds to a twisted hexagonal (TH) stacking with binding energy lowered by 2.75 kcal/mol, which is different from the situation in the benzene dimer, where rotating one monomer with respect to the other makes a rather small (less than 0.1 kcal/mol) difference to the binding energy.[62] Therefore, the energy order for different stacking orders is S (-58.02) > P (-57.03) > TH (-54.93) > H (-52.17), which is consistent with the previous calculations for coronene dimers using the DFT method with a hybrid meta exchange-correlation functional.[28] Furthermore, for both H and S stacking orders, the variations in binding energies with the interlayer rotation are only about 4 to 6%. So, it is reasonable to assume that the stacking defects that deviate from the normal S and H orders by rotation will have a minor effect on

the π-π interactions between graphene sheets, and thus the graphene sheets easily can be rotated relative to each other, which allows for the presence of many different stacking orders that are almost degenerate in energy. It is also found that the larger is the size of the graphene sheet model, the smaller is the energy change. It may be assumed that in the limit of infinite size, there is very little energy difference except exactly at the aligned non-rotated positions, like a delta-function behavior.

It is well known that the binding of π-π interacting graphene sheets is primarily due to the dispersion interaction arising from the electron correlation effect; however, the electrostatics also affect the binding energy, including the charge polarization due to the formation of bilayers and multilayers.[28] Hence, by using Mulliken population analysis, we calculated the atomic charge distributions for the $C_{54}H_{18}$ molecule and its dimers with various stacking orders. In the monomer, the charges are -0.22|e| on the hydrogen atoms, 0.04|e| on the central carbons, 0.22|e| on the carbons with saturated hydrogen atoms at the outer rim, and 0.02|e| or -0.02|e| on other carbon atoms. In the dimers with different stacking orders, we found an increase in charges on hydrogen atoms and a decrease on carbon atoms, with a slight change by about 0.004|e|, while the charges on the central carbon atoms increase to 0.05~0.08|e|. In addition, there is no difference in the charge distribution for the two monomers. Therefore, the intra- and interlayer charge transfer is expected to be negligible, and the induction interaction, due to the charge polarization effect, is considerably weaker than other terms, which is consistent with previous analyses.[27,28]

3.3 Energy gap. For the bilayer and multilayer graphene sheet models, we also investigated the energy gaps between HOMO (the highest occupied molecular orbital) and

LUMO (the lowest unoccupied molecular orbital), and their dependence on size and stacking order. It should be mentioned that, in order to calculate accurate values of the energy gap, time-consuming excited-state calculations should be performed, such as those based on the complete active space multi-configuration self-consistent field (CASSCF) method,[63] which is not practical for graphene sheet models. Furthermore, although there is great research interest in the electronic properties of PAHs and graphene sheets, neither experimental nor theoretical data from the literature are always accurate enough to allow a definite assessment of our method for predicting the energy gap of bilayer and multilayer graphene sheet models. To provide a cursory evaluation of our method, it is found that the energy gap of the coronene monomer is 2.86 eV, which is consistent with the value of 2.93 eV from previous calculations[64] and 2.91 eV from fluorescence emission experimental data.[65]

The HOMO-LUMO gaps of graphene sheet model dimers were calculated at their equilibrium interlayer separations. Table 2 provides the energies of HOMOs and LUMOs of the stacked model dimers, and Figure 5 shows the trends of the energy gaps with increasing monomer sizes for different stacking orders. It can be seen that, except for the dimers of coronene and $C_{54}H_{18}$, the energy gaps tend to decrease with increasing size of graphene sheet models for all three stacking orders, due to the higher conjugation effect with more planar hexagonal rings. This tendency coincides with the normal size dependence known for most nanoparticles, and is also consistent with the fact that the energy gaps of special GNRs decrease with increasing ribbon width, also explored by DFT-based electronic structure method.[12,66,67] Because the graphene bilayers are zero-gap semiconductors or zero-overlap semimetals,[17] the energy gap will approach zero if the

graphene sheet models become large enough while the C/H ratio approaches infinity.

It should be noted that the dimers of centrosymmetric coronene and $C_{54}H_{18}$ (D_{6h} symmetry) present larger energy gaps compared to those of the neighboring dimers consisting of smaller PAH monomers with D_{2h} symmetry. This oscillatory behavior of energy gaps may be due to the change in charge transfer caused by the change in the monomer's symmetry.[21] Therefore, unlike the strength of the π-π interaction, the energy gaps of PAH dimers depend not only on their size, but also upon the topological arrangement of hexagonal rings in the monomers. It should also be noted that the S and P stackings provide similar energy gaps, with the former being slightly larger, whereas the gaps given by H stacking are smaller by about 0.2 to 0.3 eV, and the difference almost does not change when the graphene sheet models are larger than coronene. The narrower energy gap for H stacked dimers may be due to the weaker interlayer π-π interaction, as indicated above. Taking the $C_{54}H_{18}$ dimer as an example, the energy gap given by S, P, and H stacking orders are 1.71, 1.67, and 1.52 eV, respectively. The difference of 0.19 eV between the S and H stacked dimers is smaller than that induced by the change in size. Therefore, the stacking orders have a minor effect on the variation in the HOMO-LUMO energy gap of graphene sheet model dimers.

We also investigated the dependence of energy gaps on the number of stacked graphene sheet layers. For the coronene and $C_{54}H_{18}$ models, we calculated the energy gaps of their monomer, of their trimers with ABA and ABC stacking orders, and of their tetramers with an ABAB sequence, which are shown in the insets in Figure 5. It was found that for $C_{54}H_{18}$, for example, the energy gap is reduced from 1.89 eV to 1.71 eV when two $C_{54}H_{18}$ molecules are coupled with S stacking order. The narrower energy gap of the dimer is due

to the fact that the interlayer π-π interaction leads to the degenerate HOMO and LUMO of monomers splitting into non-degenerate molecular orbitals, which results in the upshifting of the HOMO level and the downshifting of the LUMO level of the dimer relative to monomers, and thus the smaller gap. Therefore, it is also reasonable that the S and P stacked dimers show a wider energy gap than with H stacking, as mentioned above, since the π-π interactions in H stacked dimers are weaker. In addition, when a third layer is added, the decrease in the energy gap is smaller, namely 0.09 eV and 0.08 eV for ABA and ABC stacking orders, respectively. The energy gap of the ABAB stacked tetramer is reduced by only 0.03 eV compared to that of the ABA trimer. This shows that the number of graphene sheets has little effect on the energy gaps of PAH multilayers beyond the bilayer. The tendency of energy gaps to decrease with the successive addition of layers is consistent with that observed in graphene sheets.[11,68]

Furthermore, we calculated the variation in the energy gaps of $C_{54}H_{18}$ dimers with their relative rotations. We found that such rotation increases the energy gap from 1.71 eV to 1.79 eV for the S stacked dimer, while the increase is 0.14 eV for the H stacked dimer. Consequently, the difference in energy gaps of H and S stacking orders decreases from 0.19 eV to 0.13 eV. These variations in the energy gaps due to the stacking defects induced by interlayer rotation are comparable to those caused by multilayer effects. Therefore, it can be concluded that the size-dependence effect can considerably alter the energy gaps of graphene sheet model multilayers, while the changes in the stacking orders and number of stacked layers have a much weaker influence.

Finally, it is worth emphasizing that luminescence is strongly related to the HOMO-LOMO energy gap of the individual micro-units. As mentioned above, a visible

broadband luminescence between 1.5 and 2.5 eV has been observed in various CVD diamond films[20] that contain a certain amount of π-bonding sp^2 domains or graphene-like clusters, which may cause luminescence at different energy locations in accordance with their different sizes, due to the size-dependence effect of the energy gap.[21] Although graphene sheets can serve as building units for all sp^2 carbon materials, both the graphene monolayer and bilayers are known as zero-gap semiconductors. Therefore, the high-quality oriented epitaxial graphene sheets lack a large enough energy gap, and thus may not show luminescence in the range 1.5~2.5 eV generated by an optical transition between band states. Many proposals have been made to open a gap in graphene's electronic spectra, by the electric field effect,[69] lateral-superlattice potential,[68,70] and spatial confinement.[12,66] However, we find in this study that the PAHs, as molecular models of graphene sheets, show a fairly broad energy gap distribution, due mainly to the variation in their different sizes, ranging from about 1.0 to 2.5 eV. These values can be tuned by about 0.3 eV by changing the number of stacked graphene sheets and the stacking order. As mentioned above, the calculated values of the HOMO-LUMO energy gaps in this study may not be accurate enough, due to the limitation of the method and lack of reference data for comparison. Nevertheless, the tendency and the ordering of different kinds of stacked multilayers are relatively reliable, which may shed light on a promising direction for band-gap engineering of graphene sheets, GNRs, or any nanoscaled π-bonding sp^2 structures similar to graphene bilayers and multilayers. Moreover, nanomaterials consisting of π-π interacting PAH fragments may provide luminescence at various energy locations by adjusting the proportion of graphene-like clusters with a proper size distribution, as well as the stacking order and the number of stacked layers, which can be approached by proper

control of experimental parameters.

4. Summary

The π-π interaction was investigated by employing the *ab initio* DFT method, augmented by an empirical dispersion correction of R^{-6} form, which is defined by a set of empirical parameters. The method was calibrated by studying the binding energies and intermolecular distances for various configurations of benzene dimers, and comparing them with the reference data. We calculated the binding energies and energy gaps of a series of PAH dimers and multilayers of increasing size as models for stacked graphene sheets. Our results showed that the binding energies of graphene sheet model dimers are strongly dependent on the size of the PAH, on stacking order, and on the number of stacked layers. , We found a tendency for the HOMO-LUMO energy gap of PAH dimers to decrease with increasing size of the monomer, while the stacking order and successive addition of layers have a minor influence. The broad energy gap distribution, due mainly to the size-dependence effect, shows that well-designed graphene sheets, GNRs, and nanomaterials composed of π-π interacting PAH fragments will provide luminescence at different energy locations.

Acknowledgement

The work described in this paper was supported by the City University of Hong Kong [Project No. 7002030], Research Grants Council of Hong Kong SAR [project No. CityU 102707], and with computer time provided by the CityU Centre for Applied Computing and Interactive Media (ACIM).

References

1. C. A. Hunter and J. K. M. Sanders, J. Am. Chem. Soc. **112**, 5525 (1990)
2. G. R. Desiraju and A. Gavezzotti, J. Chem. Soc., Chem. Commun. **10**, 621 (1989)
3. C. A. Hunter, K. R. Lawson, J. Perkins, and C. J. Urch, J. Chem. Soc., Perkin Trans. 2 **5**, 651 (2001)
4. M. F. Brana, M. Cacho, A. Gradillas, B. Pascual-Teresa, A. Ramos, Curr. Pharm. Des. **7**, 1745 (2001)
5. A. V. Muehldorf, D. van Engen, J. C. Warner, and A.D. Hamilton, J. Am. Chem. Soc. **110**, 6561 (1988)
6. S. B. Ferguson, E. M. Sanford, E. M. Seward, and F. Diederich, J. Am. Chem. Soc. 113, 5410 (1991)
7. C. Chipot, R. Jaffe, B. Maigret, D. A. Pearlman, and P. A. Kollman, J. Am. Chem. Soc. **118**, 11217 (1996)
8. S. K. Burley and G. A. Petsko, Science **229**, 23 (1985)
9. T. Blundell, J. Singh, J. M. Thornton, S. K. Burley, and G. A. Petsko, Science **234**, 1105 (1986)
10. P. Hobza, H. L. Selzle, and E. W. Schlag, Chem. Rev. **94**, 1767 (1994)
11. K. S. Novoselov, A. K. Geim, S. V. Morozov, D. Jiang, Y. Zhang, S. V. Dubonos, I. V. Gregorieva, and A. A. Firsov, Science **306**, 666 (2004)
12. V. Barone, O. Hod, and G. E. Scuseria, Nano Lett **6**, 2748 (2006)
13. K. S. Novoselov, E. McCann, S. V. Mozorov, V. I. Fal'ko, M. I. Katsnelson, U. Zeitler, D. Jiang, F. Schedin, and A. K. Geim, Nat. Phys. **2**, 177 (2006)
14. E. McCann and V. I. Fal'ko, Phys. Rev. Lett. **96**, 086805 (2006)
15. L. M. Malard, J. Nilsson, D. C. Elias, J. C. Brant, F. Plentz, E. S. Alves, A. H. Castro Neto, and M. A. Pimenta, Phys. Rev. B **76**, 201401 (2007)
16. A. H. Castro Neto, F. Guinea, N. M. Peres, K. S. Novoselov, and A. K. Geim, Rev. Mod. Phys. **81**, 109 (2009)
17. A. K. Geim and K. S. Novoselov, Nature **6**, 183 (2007)
18. J. S. Wu, W. Pisula, and K. Muellen, Chem. Rev. **107**, 718 (2007)
19. U. P. Vijh, A. D. Witt, and K. D. Gordon, Astrophysical Journal **606**, 65 (2004)
20. P. Kania, and P. Oelhafen, Diamond Relat. Mater **4**, 425 (1995)

21. R. Q. Zhang, E. Bertran, and S. T. Lee, Diamond and Related Materials **7**, 1663 (1998)
22. Z. Liu, K. Suenaga, P. J. F. Harris, and S. Iijima, Phys. Rev. Lett. **102**, 015501 (2009)
23. M. O. Sinnokrot, and C. D. Sherrill, J Phys Chem A **110**, 10656 (2006)
24. S. Latil and L. Henrard, Phys. Rev. Lett. **97**, 036803 (2006)
25. M. Aoki and H. Amawashi, Solid State Comm. **142**, 123 (2007)
26. F. Guinea, A. H. Castro Neto, and N. M. R. Peres, Solid State Comm. **143**, 116 (2007)
27. S. Grimme, C. Mück-Lichtenfeld, and J. Antony, J. Phys. Chem. C **111**, 11199 (2007)
28. Y. Zhao and D. G. Truhlar, J. Phys. Chem. C **112**, 4061 (2008)
29. S. Tsuzuki, Struc. Bond **115**, 149 (2005)
30. S. Kristyán and P. Pulay, Chem. Phys. Lett. **229**, 175 (1994)
31. S. Grimme, J. Comput. Chem. **25**, 1463 (2004)
32. E. J. Meijer and M. Sprik, J. Chem. Phys. **105**, 8684 (1996)
33. W. T. M. Mooij, F. B. van Duijneveldt, J. G. C. M. van Duijneveldt-van de Rijdt, B. P. van Eijck, J. Phys. Chem. A **103**, 9872 (1999)
34. M. Elstner, P. Hobza, Th. Frauenheim, S. Suhai, and E. Kaxiras, J. Chem. Phys. **114**, 5149 (2001)
35. X. Wu, M. C. Vargas, S. Nayak, V. Lotrich, and G. Scoles, J. Chem. Phys. **115**, 8748 (2001)
36. Q. Wu and W. Yang, J. Chem. Phys. **116**, 515 (2002)
37. U. Zimmerli, M. Parrinello, and P. Koumoutsakos, J. Chem. Phys. **120**, 2693 (2004)
38. R. Peverati and K. K. Baldridge, J. Chem. Theory. Comput. **4**, 2030 (2008)
39. M. Elstner, D. Porezag, G. Jungnickel, J. Elsner, M. Haugk, Th. Frauenheim, S. Suhai, and G. Seifert, Phys. Rev. B **58**, 7260 (1998)
40. C. S. Lin, R. Q. Zhang, S. T. Lee, M. Elstner, T. Frauenheim, and L. J. Wan, J Phys Chem B **109**, 14183 (2005)
41. C. Feng, C. Zhang, R. Q. Zhang, T. Frauenheim, M. A. van Hove, J. Phys.: Cond. Matter **20**, 275240 (2008)
42. P. Ordejón, E. Artacho, and J. M. Soler, Phys Rev B **53**, R10441 (1996)
43. J. M. Soler, E. Artacho, J. D. Gale, A. García, J. Junquera, P. Ordejón, and D. Sánchez-Portal, J. Phys. Condes.: Matter **14**, 2745 (2002)

44. P. Hobza, H. L. Selzle, and E. W. Schlag, J. Chem. Phys. **100**, 18790 (1996)
45. S. Tsuzuki, K. Honda, M. Mikami, and K. Tanabe, J. Am. Chem. Soc. **124**, 104 (2002)
46. M. O. Sinnokrot, E. F. Valeev, amd C. D. Sherrill, J. Am. Chem. Soc. **124**, 10887 (2002)
47. M. O. Sinnokrot and C. D. Sherrill, J. Phys. Chem. A **110**, 10656 (2006)
48. J. G. Hill, J. A. Platts, and H. J. Werner, Phys. Chem. Chem. Phys. **8**, 4072 (2006)
49. E. C. Lee, D. Kim, P. Jurečka, P. Tarakeshwar, P. Hobza, and K. S. Kim, J. Phys. Chem. A **111**, 3446 (2007)
50. R. A. Jr Distasio, G. von Helden, R. P. Steele, and M. Head-Gordon, Chem. Phys. Lett. **437**, 277 (2007)
51. M. Pitoňák, R. Neogrády, J. Řezáč, P. Jurekča, M. Urban, and P. Hobza, J. Chem. Theory Comput. **4**, 1829 (2008)
52. T. Janowski and P. Pulay, Chem. Phys. Lett. **447**, 27 (2007)
53. C. Feng, C. S. Lin, X. H. Zhang, and R. Q. Zhang, J. Theor. Comput. Chem., *to be published* (2009)
54. X. Gonze, J. M. Beukn, R. Caracus, Comput. Matter Sci. **25**, 478 (2002)
55. Y. X. Zhao and I. L. Spain, Phys. Rev. B: Condens. Matter Mater. Phys. **40**, 993997 (1989)
56. M. S. Dresselhaus and G. Dresselhaus, Adv. Phys. **51**, 1 (2002)
57. H. Ruuska and T. A. Pakkanen, J. Phys. Chem. B **105**, 9541 (2001)
58. T. Dahl, Acta. Chem. Scand. **48**, 95 (1994)
59. A. G. Donchev, Phys. Rev. B **74**, 235401 (2006)
60. F. Guinea, A. H. Castro.Neto, and N. M. R. Peres, Phys. Rev. B **73**, 245426 (2006)
61. E. Cisternas, M. Flores, and P. Vargas, Phys. Rev. B **78**, 125406 (2008)
62. R. L. Jaffe, and G. D. Smith, J. Chem. Phys. **105**, 2780 (1996)
63. J. D. Kubicki, G. A. Blake, and S. E. Apitz, Environ. Toxicol. Chem. **18**, 1656 (1999)
64. Y. Ruiz-Morales, J Phys Chem A **106**, 11283 (2002)
65. W. E. Jr. Acree and S. A. Tucker, Polycyclic Aromat. Compd. **2**, 75 (1991)
66. M. Y. Han, B. Özyilmaz, Y. Zhang, and P. Kim, Phys. Rev. Lett. **98**, 206805 (2007)
67. B. Sahu, H. Min, A. H. MacDonald, and S. K. Banerjee, Phys. Rev. B **78**, 045404 (2008)

68. S. Y. Zhou, G. H. Gweon, and A. V. Fedorov, Nature Materials **6**, 770 (2007)
69. E. V. Castro, K. S. Novoselov, S. V. Morozov, N. M. R. Peres, J. M. B. Lopes Dos Santos, Nilsson Johan, F. Guinea, A. K. Geim, and A. H. Castro Neto, Phys. Rev. Lett. **99**, 216802 (2007)
70. T. Ohta, A. Bostwick, T. Seyller, K. Horn, and E. Rotenberg, Science **313**, 951, (2006)

Table 1. Binding energies per layer (in kcal/mol) for the centrosymmetrical $C_{24}H_{12}$ and $C_{54}H_{18}$ with different numbers of layers and different stacking orderings.

Stacking sequence	Number of layers	$C_{24}H_{12}$	$C_{54}H_{18}$
AB	2	-22.64	-58.02
ABA	3	-23.02	-58.71
ABC	3	-22.99	-58.53
ABAB	4	-23.18	-58.37

Table 2. Energies of HOMOs and LUMOs of various graphene sheet model dimers for the staggered, hexagonal, and parallel-displaced stackings, respectively, along with those of $C_{24}H_{12}$ and $C_{54}H_{18}$ trimers with ABA and ABC stackings, and tetramers with an ABAB sequence. (Unit is eV)

	Staggered		Hexagonal		Parallel-displaced		ABA	ABC	ABAB
	HOMO	LUMO	HOMO	LUMO	HOMO	LUMO			
$C_{16}H_{10}$	-4.659	-2.191	-4.573	-2.367	-4.679	-2.300			
$C_{24}H_{12}$	-4.797	-2.152	-4.725	-2.253	-4.772	-2.166	-4.615/ -2.116	-4.681/ -2.135	-4.678/ -2.142
$C_{32}H_{14}$	-4.485	-2.716	-4.302	-2.767	-4.364	-2.611			
$C_{42}H_{16}$	-4.305	-2.810	-4.192	-2.948	-4.316	-2.884			
$C_{54}H_{18}$	-4.467	-2.761	-4.374	-2.844	-4.440	-2.767	-4.380/ -2.750	-4.379/ -2.759	-4.338/ -2.745
$C_{66}H_{20}$	-4.262	-3.131	-4.100	-3.235	-4.247	-3.240			
$C_{80}H_{22}$	-4.210	-3.216	-4.069	-3.352	-4.193	-3.336			

Figure Captions

Figure 1. Structures of a series of PAH models for graphene sheets: (a) $C_{16}H_{10}$, (b) $C_{24}H_{12}$, (c) $C_{32}H_{14}$, (d) $C_{42}H_{16}$, (e) $C_{54}H_{18}$, (f) $C_{66}H_{20}$, and (g) $C_{80}H_{22}$. The terminal bonds indicate the sites of boundary hydrogen atoms.

Figure 2. Top views of the arrangement of the carbon atoms in two adjacent coronene planes in (a) staggered and (b) parallel-displaced stacking, and in coronene trimers with (c) ABA and (d) ABC stacking; grey, red and blue represent the lowest, middle and top layer, respectively.

Figure 3. Binding energy per carbon atom for graphene sheet model dimers of different sizes. The solid, dashed, and dotted lines represent the staggered, hexagonal, and parallel-displaced stackings, respectively.

Figure 4. Variation of binding energies of a $C_{54}H_{18}$ dimer with the rotation angle between the two layers, relative to its normal S and H stacking orderings.

Figure 5. Variation of the energy gap with the size of graphene sheet model dimers for the staggered, hexagonal, and parallel-displaced stackings, respectively. The open symbols and the insets show the energy gaps of $C_{24}H_{12}$ and $C_{54}H_{18}$ monomers, and their trimers with ABA and ABC stackings, and tetramers with an ABAB sequence.

(a)

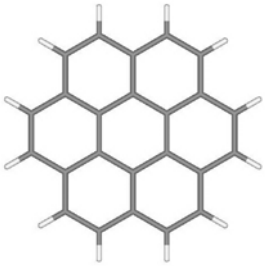

(b)

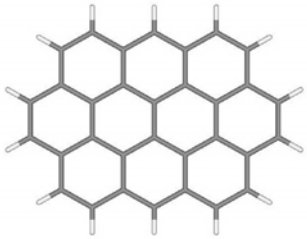

(c)

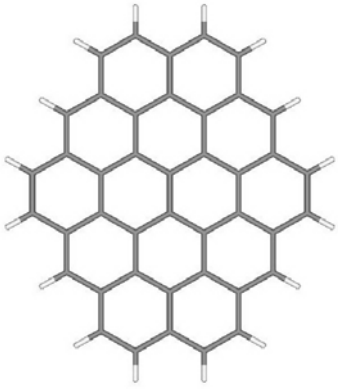

(d)

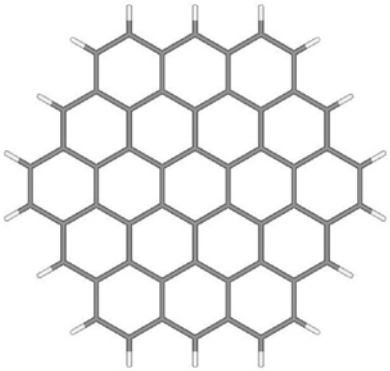

(e)

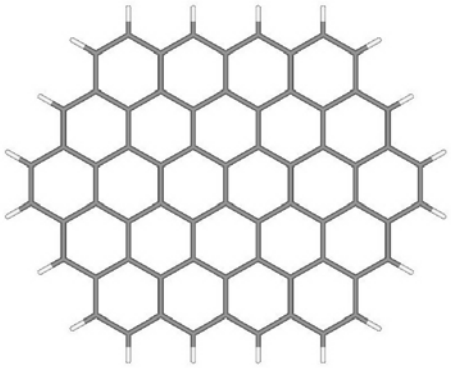

(f)

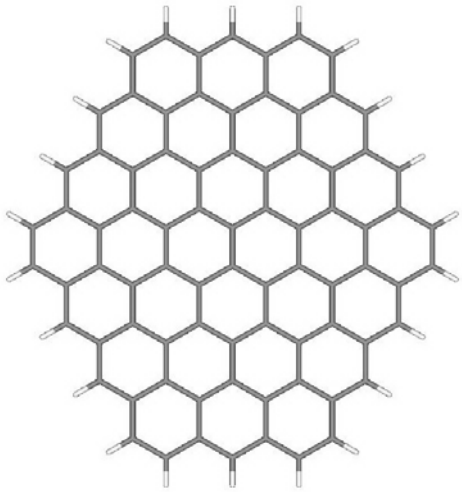

(g)

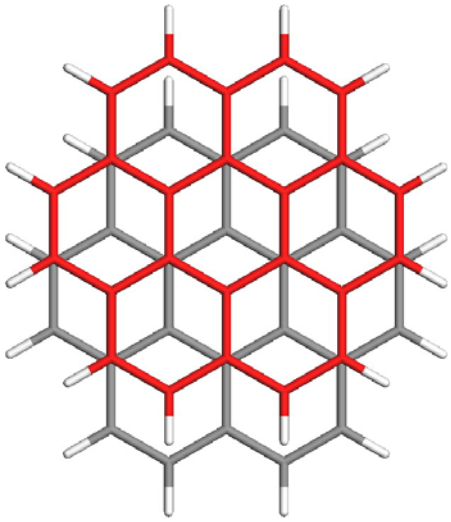

(a)

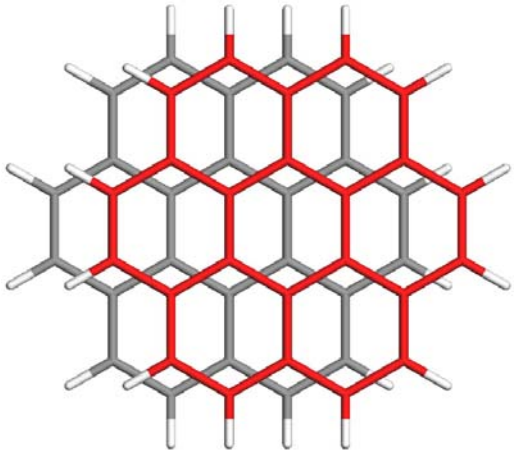

(b)

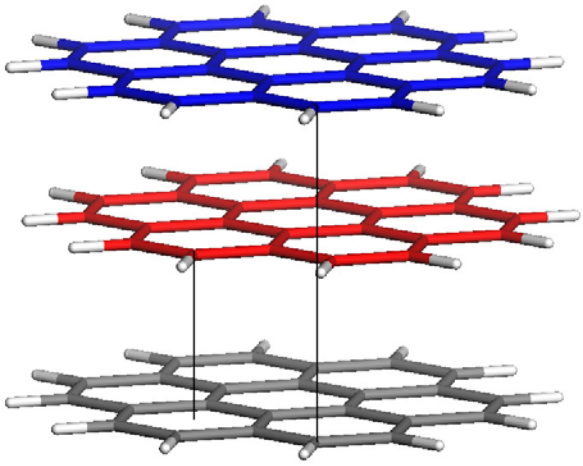

(c)

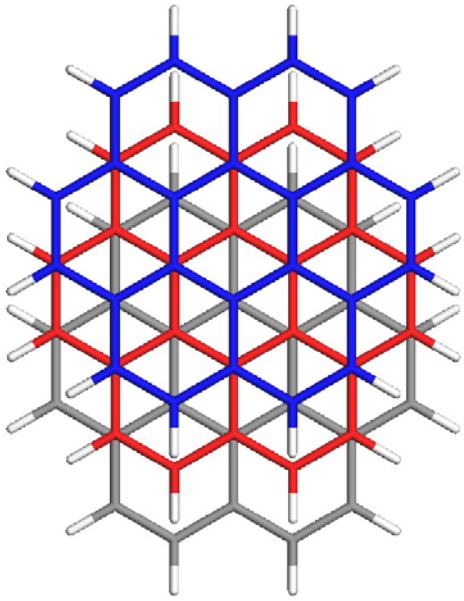

(d)

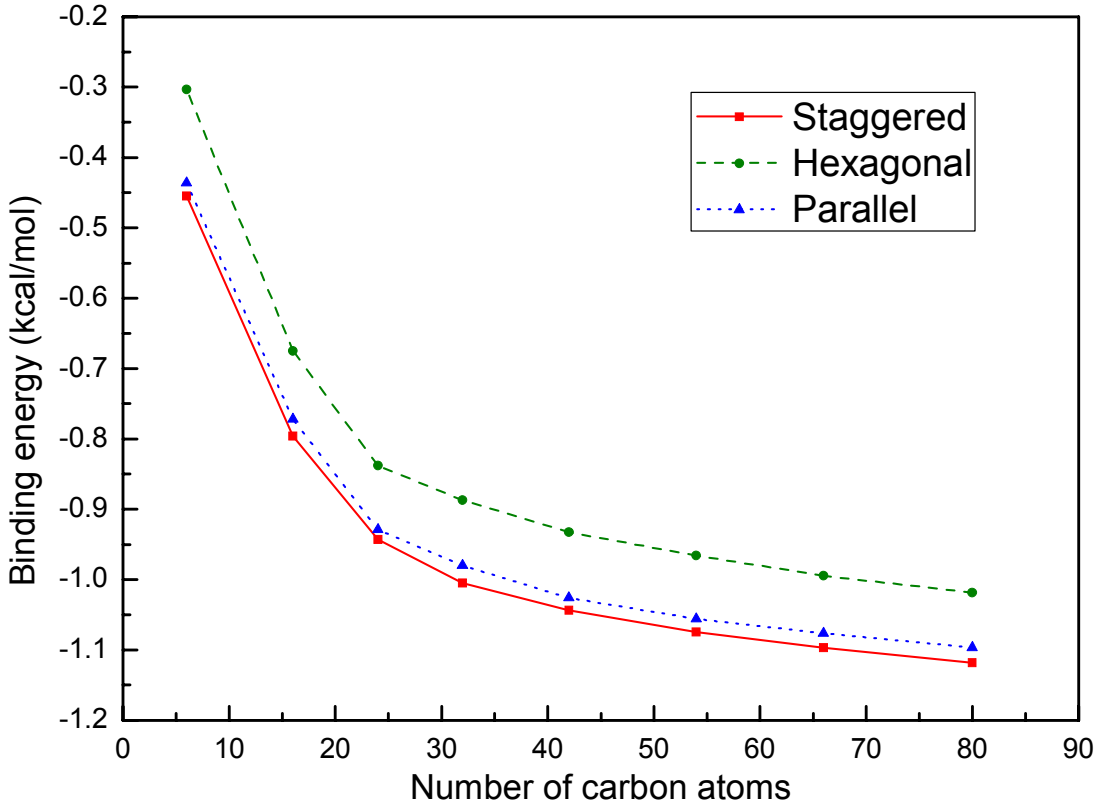
Staggered
Hexagonal
Parallel
Binding energy (kcal/mol)
-0.2
-0.3
-0.4
-0.5
-0.6
-0.7
-0.8
-0.9
-1.0
-1.1
-1.2
0
10
20
30
40
50
60
70
80
90
Number of carbon atoms

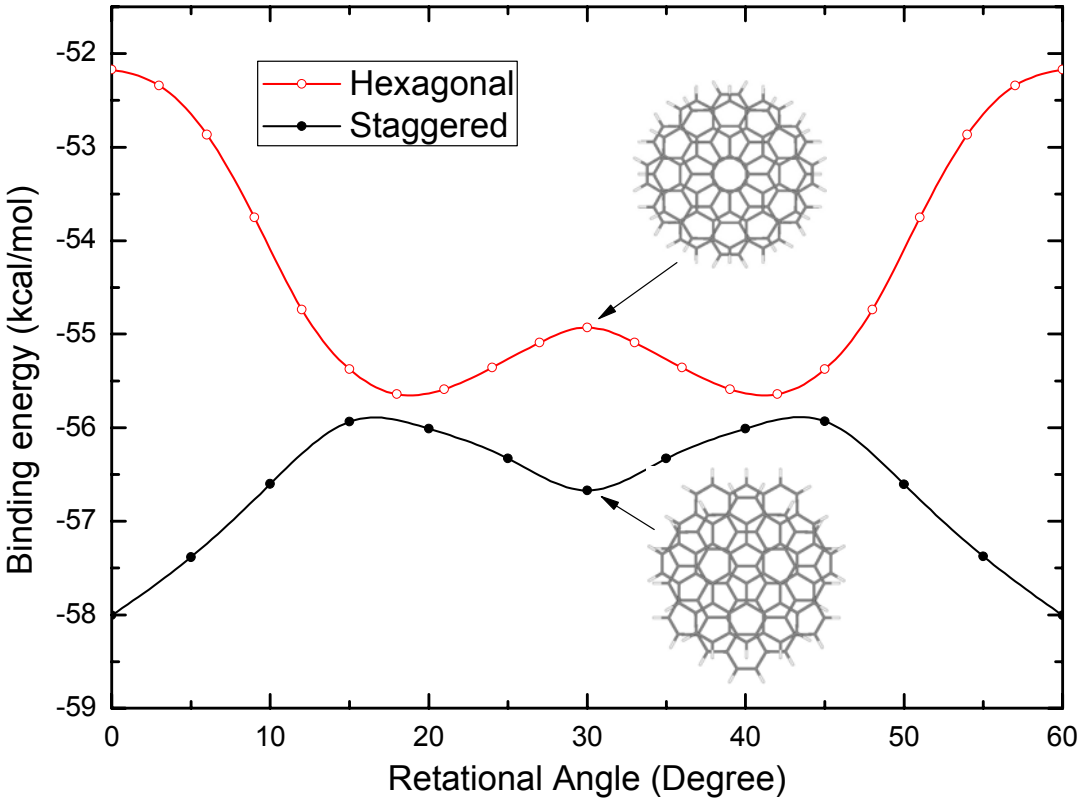
Hexagonal
Staggered
Binding energy (kcal/mol)
-52
-53
-54
-55
-56
-57
-58
-59
0
10
20
30
40
50
60
Retational Angle (Degree)

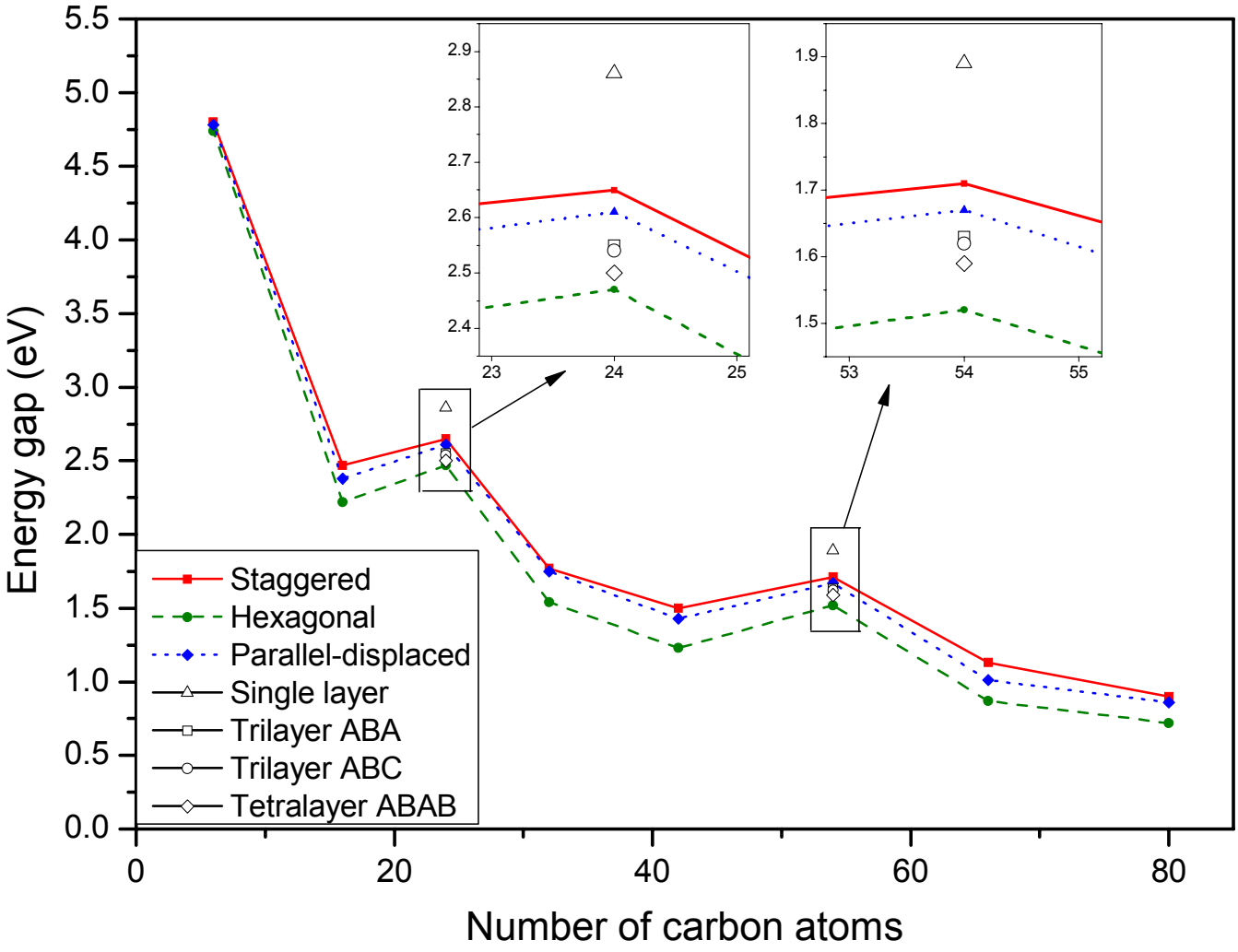
Energy gap (eV)
Number of carbon atoms
Staggered
Hexagonal
Parallel-displaced
Single layer
Trilayer ABA
Trilayer ABC
Tetralayer ABAB